Detailed characterization of CW- and pulsed-pump four-wave mixing in highly nonlinear fibers

Lillieholm, Mads; Galili, Michael; Grüner-Nielsen, L.; Oxenløwe, Leif Katsuo

Published in:
Optics Letters

Link to article, DOI:
10.1364/OL.41.004887

Publication date:
2016

Document Version
Peer reviewed version

Detailed Characterization of CW- and Pulsed-Pump Four-Wave Mixing in Highly Nonlinear Fibers

M. LILLIEHOLM,[1,*] M. GALILI,[1] L. GRÜNER-NIELSEN[2] AND L. K. OXENLØWE[1]

[1]DTU Fotonik, Dept. of Photonics Engineering, Technical University of Denmark, Ørsteds Plads Bldg. 343, DK-2800 Kgs. Lyngby, Denmark
[2]OFS, Priorparken 680, DK-2605, Brøndby, Denmark
*Corresponding author: madsl@fotonik.dtu.dk

Received XX Month XXXX; revised XX Month, XXXX; accepted XX Month XXXX; posted XX Month XXXX (Doc. ID XXXXX); published XX Month XXXX

We present a quantitative comparison of continuous-wave- (CW) and pulsed-pump four-wave mixing (FWM) in commercially available highly nonlinear fibers (HNLFs), and suggest properties for which the CW and pulsed FWM bandwidths are limited in practice. The CW- and pulsed-pump parametric gain is characterized experimentally for several HNLFs with various dispersion properties, including zero-dispersion wavelength fluctuations, and the results are interpreted in conjunction with detailed numerical simulations. It is found that a low third order dispersion (TOD) is essential for the pulsed-pump FWM bandwidth. However, an inverse scaling of the TOD with the dispersion fluctuations, leads to different CW-optimized fibers, which depend only on the even dispersion-orders.

OCIS codes: *(060.4370) Nonlinear optics, fibers; (190.4380) Nonlinear optics, four-wave mixing; (260.2030) Dispersion.*

http://dx.doi.org/10.1364/OL.99.099999

Four-wave mixing (FWM) in highly nonlinear fibers (HNLFs) [1] has been proven to enable a number of important functionalities for ultrafast optical signal processing (OSP). For continuous-wave (CW) pumps such OSP includes fiber-optic parametric amplifiers [2] and optical phase conjugation [3,4], whereas broadband pulsed pumps enable e.g. sub-picosecond resolution optical sampling [5] and optical Fourier transformation [**Error! Reference source not found.**,7] based on the optical time lens principle [8]. It is possible to achieve very high efficiency in HNLFs [9] and FWM bandwidths have been reported up to 140 nm using a CW pump [10] which in principle depends only on the even dispersion orders [11]. However, the pulsed-pump performance is rarely characterized. The fiber requirements for pulsed-pump FWM (pulsed FWM) in HNLFs are generally more demanding than for CW-pumped FWM (CW FWM), with tolerances decreasing for larger pump bandwidths due to walkoff, which is often limited by the third order dispersion (TOD) for a fixed length of fiber. Another consequence of TOD is for chirped pump pulses, where the phase matching conditions change depending on which part of the pump spectral content is overlapping with the signal temporally, as is the case in e.g. a FWM-based time lens. Finally, the strength of Raman interactions may vary considerably depending on the type and concentration of the fiber core dopants [12], affecting the Raman-induced frequency shift for ultrashort pulsed-pump FWM. In this letter we compare a range of HNLF types with different dispersion properties, to characterize their potential for CW and pulsed FWM respectively. As part of the characterization, the parametric gain is measured on standard HNLF, dispersion-flattened HNLF (DF-HNLF) and for different variations of the highly dispersion-stable HNLF-SPINE [13]. To complement the experimental results, a detailed numerical fiber model is used to simulate the CW and pulsed fiber performance for varied dispersion parameters, including the Raman effect and estimation of the zero-dispersion wavelength (ZDW) fluctuations. It is suggested that fundamental differences between the fibers are related to the dynamic between the dispersion slope and ZDW fluctuations, which make fibers with a relatively large dispersion slope potentially more suitable for high performance CW FWM, whereas fibers with a low dispersion slope are promising for pulsed FWM applications.

The primary frequency dependence, and hence bandwidth limitation, of the FWM process is due to the linear phase mismatch $\Delta\beta$. Note that herein it is assumed that the bandwidth is not limited by polarization-mode dispersion (PMD) [14,15]. When expanded around the pump frequency, ω_p, the phase mismatch is [11]:

$$\Delta\beta \approx \beta_2(\omega_s-\omega_p)^2+\frac{\beta_4}{12}(\omega_s-\omega_p)^4. \qquad (1)$$

Here β_2 and β_4 are the second and fourth order fiber dispersion coefficients at the pump frequency respectively, ω_s is the signal frequency and higher order terms have been neglected. Hence, the phase mismatch dependence on the fiber stems from β_2 and β_4. As β_2 can be tuned by moving the pump frequency and β_4 is assumed relatively constant within a practical bandwidth, the optimization procedure is straightforward [11], although it is complicated somewhat by the inclusion of the nonlinear phase term. For pulsed-pump FWM, walkoff must be considered; even for a CW

input signal where there in principle is no pump-signal walkoff, as the resulting pump-idler walkoff affects the FWM bandwidth similarly to pump-signal walkoff. For the conventional method of phase mismatch minimization which places the pump near the ZDW, the walkoff increases with the pump-signal wavelength detuning. Thus, the bandwidth is limited to the point where the walkoff approaches the pump pulse-duration, regardless of the phase mismatch. Unlike the phase mismatch due to dispersion, which depends only on even dispersion orders, the walkoff additionally depends on the odd. Expansion of the group delay, $\beta_1 L$, around the pump frequency leads to the pump-signal walkoff Δt_{wo}:

$$\Delta t_{wo} \approx \left[\beta_2(\omega_s - \omega_p) + \frac{\beta_3}{2}(\omega_s - \omega_p)^2 + \frac{\beta_4}{6}(\omega_s - \omega_p)^3 \right] L, \quad \textbf{(2)}$$

which shows the added dependence on the TOD, β_3, for pulsed FWM in a fiber of length L. As $\beta_2(\omega_p)$ is kept small in practice, the walkoff will typically be dominated by the β_3-term for a fixed fiber length. As a special case, the temporally local interaction for chirped pump pulses is narrowband compared to the pump bandwidth, $\Delta\omega_p$, and the FWM efficiency depends on the phase mismatch for individual spectral pump components. Hence, β_2 may vary by up to $\Delta\beta_2 = \Delta\omega_p\beta_3$, which can limit the bandwidth in e.g. a time lens system using a HNLF with large β_3 or a large pump bandwidth, which has been demonstrated up to 1.6 THz [16].

To test our assumption that pulsed FWM is sensitive to β_3, whereas CW FWM depends only on β_2 and β_4, the parametric gain for both CW and pulsed FWM is measured for four different 500-m fibers, with an order of magnitude difference between the highest and lowest dispersion slope at the ZDW, S_0 ($\propto \beta_3$). Table 1 lists relevant parameters for the fibers under test (FUT) with assigned IDs A to D. Fiber A is a DF-HNLF, B is a standard HNLF, C is the HNLF-SPINE and D is a variation on the HNLF-SPINE, engineered to lower the value of β_4 (HNLF-SPINE $\beta_4\downarrow$). The dispersion parameters have been derived from a five-term Sellmeier polynomial fitted to the group delay [17], which was measured using an Agilent 86037C dispersion test set. Fig. 1(a) shows a schematic diagram of the experimental setup, with the pulsed waveform traces shown as an inset. Fig. 1(b) shows the significantly different pulsed FWM spectra for fibers A and C. For the CW characterization, the pump is generated from an external cavity laser (ECL) source, then phase modulated using four radio-frequency tones to suppress stimulated Brillouin scattering [18], and amplified to obtain 28 dBm average power after a 0.8-nm

Table 1. Parameters for highly nonlinear fibers under test.

ID	λ_0 [nm]	S_0 [ps/(nm^{2}km)]	β_4 [ps^4/km]
A	1541.3	0.0074	2.6×10^{-4}
B	1546.7	0.017	1.3×10^{-4}
C	1542.9	0.072	-3.0×10^{-4}
D	1545.4	0.070	-1.1×10^{-4}
D-PM*	1562.2	0.069	-0.93×10^{-4}
ID	L [m]	α [dB/km]	γ [W^{-1}km^{-1}]
A	506	0.76	10.8
B	500	0.74	11.3
C	508	0.83	9.7
D	498	0.47	6.7
D-PM*	497	0.49	6.7

*D-PM is a polarization-maintaining version of D used to test the accuracy of the scalar numerical model.

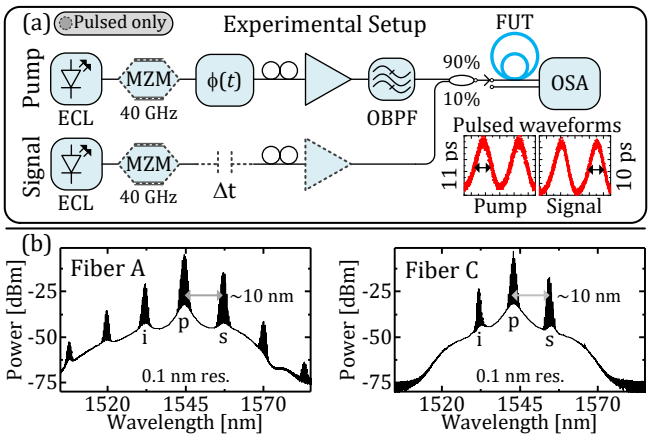

Fig. 1. Experimental setup for CW- and pulsed-pump parametric gain measurements. The inset shows the pulsed waveforms (a). Selected pulsed FWM spectra, indicating **p**ump, **s**ignal and **i**dler (b).

Gaussian optical bandpass filter (OBPF) at the input to the FUT. The signal source is an ECL launching -12 dBm power into the FUT. 40-GHz Mach-Zehnder modulators (MZMs) are inserted after the ECLs for the pulsed characterizations, to carve out 50% duty cycle pulses with 11 ps full-width at half maximum (FWHM). The pulsed pump is amplified to 25 dBm average power at the FUT input after a 3-nm Gaussian OBPF, to obtain a peak power comparable to the CW pump power. The average pulsed signal power is amplified to 0 dBm, thus increasing the detected idler power at the attenuated optical spectrum analyzer (OSA), which is low in some cases. No gain saturation was observed. The parametric gain is defined as the ratio of the signal power at the output to the signal power at the input of the FUT, and the signal power is calculated by integrating over the signal spectrum, measured using the OSA. For pulsed measurements, the delay and polarization was optimized for each point, whereas fast tunable laser sweeps were used for the CW measurements, with the polarization optimized for $\lambda_s = 1550$ nm. Fig. 2 shows the parametric gain as a function of the pump-signal detuning for fibers A to D. For A and B with low slopes, the pulsed gain spectrum closely resembles the CW gain spectrum. For C and D with larger slopes, the pulsed gain drops off for a detuning >20 nm compared to the CW gain, supporting that the value of the TOD significantly impacts the pulsed performance.

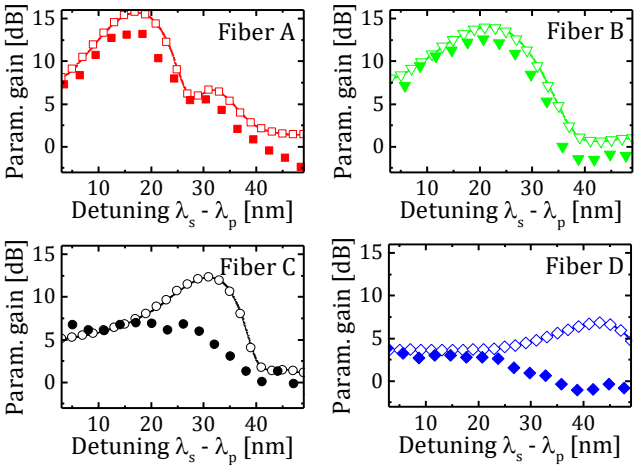

Fig. 2. The CW- (open symbols) and pulsed-pump (solid symbols) parametric gain measured for fibers A-D with λ_p at 1547.53 nm, 1548.30 nm, 1542.86 nm and 1545.32 nm respectively.

Fluctuations of the ZDW add a z-dependence for $\beta_2(\omega_p, z)$ which limits the FWM bandwidth via $\Delta\beta$. Hence, as a further characterization of the fibers, the average ZDW was measured on several adjacent pieces from the same preforms, with lengths ranging from ~0.1 km to ~1 km, resulting in low-resolution ZDW maps over ≥6 km for the different HNLF variations, shown in Fig. 3. Even for a modest resolution, very large differences can be observed for the different HNLF variations. The DF-HNLF exhibits ZDW fluctuations up to 52 nm, the standard HNLF up to 9 nm and 1.3-1.4 nm is observed for the standard HNLF-SPINE and the HNLF-SPINE $\beta_4\downarrow$. The origin of the differences lies mainly with the effect of core-radius fluctuation artifacts from the fiber drawing process on the dispersion, which can be approximately modeled as a vertical translation of the β_2 vs. frequency curve [19]. The simplified model is illustrated in Fig. 4(a) for two different dispersion slopes, $S > 0$. For $S = x$ (low β_3) the incremental ZDW fluctuation $\delta\lambda_0$ is doubled compared to $S = 2x$ (high β_3), for the same incremental dispersion (β_2) change δD. As a consequence, controlling the ZDW in the direction of propagation is extremely challenging for DF-HNLFs in particular. Conversely, for a fixed ZDW fluctuation the change in dispersion is proportional to the dispersion slope. For this model, the relation $\delta D = S\delta\lambda_0$, can be used to express a first order approximation for the variation of $\Delta\beta$, $\delta\beta = -2\pi c\delta D \times (\lambda_p/\lambda_s - 1)^2$. Based on the observed data, the fluctuations may increase faster than the slope decreases, suggesting that $\delta\beta$ is minimized for higher slope values.

To complement the experimental findings, a detailed scalar numerical fiber propagation model was created, including ZDW fluctuations and the Raman effect. The model solves the generalized nonlinear Schrödinger equation using a 4th order Runge-Kutta in the interaction picture (RK4IP) method [20], with an adaptive step size [21]. The Raman response function is implemented using the model proposed by Lin and Agrawal [**Error! Reference source not found.**] and the Raman fraction, f_R, is reduced by approximately 20% compared to pure silica, to match the weighted GeO_2 (germania) concentration of ~20 mol % for the tested HNLFs [10]. Note that the Raman response herein overestimates the gain for a >15 THz Raman frequency shift. This is compensated by using $f_R = 0.245$ for silica instead of the typical value of $f_R = 0.18$, to yield accurate results in the 0-15 THz range [22]. Hence, the germania-modified

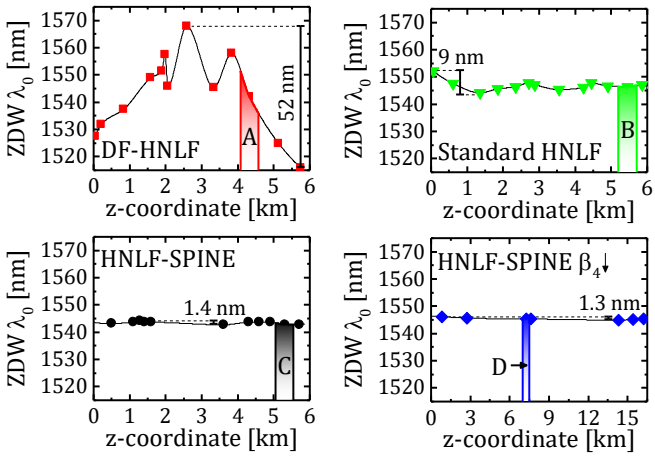

Fig. 3. ZDW maps of the different tested HNLF variations from ZDW measurements (symbols), with the positions for fibers A to D indicated on each of the graphs. Lines are shape-preserving cubic polynomial fits.

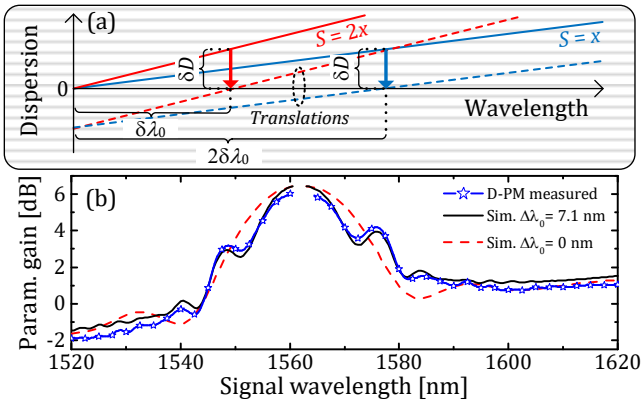

Fig. 4. Illustration of dispersion changes on the ZDW due to core radius variations for different dispersion slopes (a). Measured and simulated parametric gain spectra for test fiber D-PM (λ_p = 1561.9 nm) (b).

Raman fraction is $f_R \cong 0.2$. The ZDW fluctuations are modeled by modifying the linear dispersion operator for each step, according to the change due to the translated β_2 at the reference frequency. In general, the ZDW fluctuations are assumed to follow stochastic processes, with independent variations on both short (<1 m) and longer length scales in reality [23]. However, for the following the simple z-dependent linear variation $\lambda_0(z) = \Delta\lambda_0(z/L - 1/2) + \lambda_{0,avg}$ is used, which was found to reliably predict experimental gain spectra with minor non-reciprocal behavior. The ZDW fluctuations, $\Delta\lambda_0$, was fitted to match one of several measured gain spectra. This first order approximation of the fluctuations may be useful because fluctuations on a short scale do not significantly impact the gain spectrum in practice [23]. Whereas $\Delta\lambda_0$ cannot be attributed an exact physical significance, it is expected to be correlated with the magnitude of the random fluctuations on a long length scale. To test the model, the CW parametric gain spectrum was measured for a polarization-maintaining (PM) variant of fiber D (D-PM, cf. Table 1) with a polarization extinction ratio of 21 dB. The measured parametric gain at 28 dBm pump power, and the simulated gain for $\Delta\lambda_0 = 7.1$ nm, are shown in Fig. 4(b), indicating extremely good agreement between the experimental and simulated results. As a reference, the simulated gain spectrum for $\Delta\lambda_0 = 0$ nm is shown without the detailed

oscillations exhibited by the experimental gain spectrum. The best $\Delta\lambda_0$-fit is larger than expected for a version of the HNLF-SPINE (cf. Fig. 3), however an adjacent length of fiber from the same preform was measured to have $\lambda_0 = 1555$ nm ($\lambda_0 = 1562.2$ nm for fiber D-PM), which supports that the fluctuations are relatively large. It is supposed that the insertion of stress rods to induce birefringence destabilizes the dispersion. The simulation model was similarly used to estimate the ZDW fluctuations for fibers A to D, by selecting values of $\Delta\lambda_0$ which simultaneously achieve the best parametric gain spectrum fit at one pump wavelength, and enable the reproduction of other gain spectra for the same fiber. The results are listed in Table 2, indicating reasonable ZDW fluctuation estimates compared to the experimental measurements shown in Fig. 3. To investigate the parametric gain behavior for varying dispersion slopes, CW and pulsed FWM was simulated using the fiber parameters of D as a basis, including the estimated dispersion fluctuations. The simulated pump and signal pulses are ideal MZM-carved 50% duty cycle pulses synchronized at the fiber input, with a 40 GHz repetition rate, 12.5 ps FWHM and 28 dBm peak power.

Table 2. List of best simulated $\Delta\lambda_0$ fits.

A	B	C	D	D-PM
13 nm	4.8 nm	0.30 nm	0.16 nm	7.1 nm

The slope is varied from 0.01 to 0.09 ps/(nm^{2}km), and the pump wavelength is changed to maintain the phase matching conditions by keeping a constant average β_2 of $\sim 7 \times 10^{-3}$ ps^2/km. The simulated parametric gain spectra, normalized with respect to the gain near the pump wavelength, are shown in Fig. 5, with the experimental measurements as references. It can be seen that the CW peak gain changes by <1 dB for different dispersion slopes with constant β_2. The variations are mainly due to the fixed value of $\Delta\lambda_0 = 0.16$ nm, which impacts the gain more strongly for larger slopes. For pulsed FWM, the gain bandwidth is close to the CW bandwidth with a slope of 0.01 ps/(nm^{2}km), whereas the gain bandwidth rapidly diminishes for larger slopes. Fig. 5(b) shows the corresponding pump-signal walkoff for the different slope values, with the pump half-width at half maximum (HWHM) indicated as a suggested threshold for negligible walkoff. The HWHM is chosen instead of the FWHM since the pump and signal pulses are aligned at the input. The gain peaks present for CW FWM at a detuning of ~45 nm, vanish for slopes ≥0.03 ps/(nm^{2}km) where the walkoff exceeds the pump HWHM, thus explaining the significant differences. A slope of ~0.03 ps/(nm^{2}km) is common for good HNLFs, and yet it can result in significant bandwidth limitations for pulsed FWM in a 500-m HNLF for a modest walkoff tolerance <10 ps. The walkoff can be reduced by choosing shorter lengths of fiber, but that may not be feasible if a certain parametric gain or conversion efficiency is required for the application. On the other hand, the slope does not affect the bandwidth for CW- pumped FWM, and it may be that superior performance can be obtained in high-slope HNLFs due to increased dispersion stability, which appears to scale favorably with the dispersion slope.

In conclusion, we have measured the parametric gain using CW and pulsed pumps for different HNLF variations. Large bandwidth penalties were observed for a pulsed pump compared to a CW pump, in 500-m HNLFs with dispersion slope values of ~0.07 ps/(nm^{2}km). Conversely, the pulsed gain spectrum

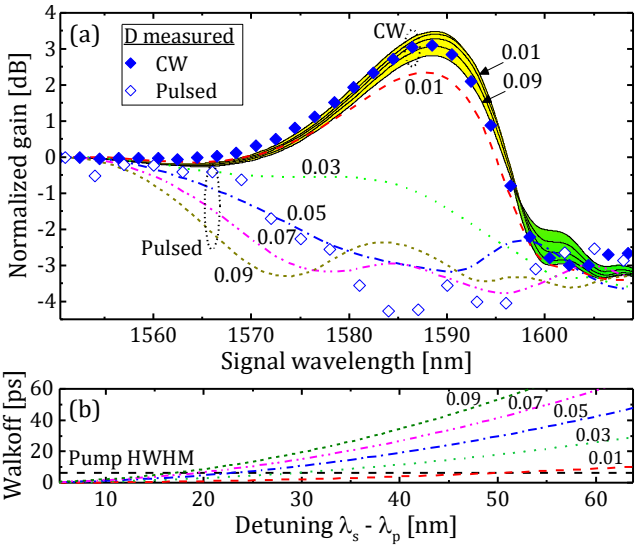

Fig. 5. Simulated CW and pulsed parametric gain spectra for the dispersion slope varied from 0.01 to 0.09 ps/(nm^{2}km). Symbols reference experimental results for fiber D (a). Pump-signal walkoff for various dispersion slopes as a function of pump-signal detuning (b).

resembles the CW gain spectrum for slopes <0.02 ps/(nm^{2}km) and a detuning of up to ~50 nm. Detailed numerical simulations were used to estimate the zero-dispersion wavelength fluctuations for different fibers, and to verify that the differences between the CW and pulsed FWM bandwidth depend mainly on the walkoff due to the dispersion slope. Zero-dispersion wavelength fluctuation measurements indicate that the fluctuations increase faster than the dispersion slope decreases. Hence, it is suggested that the optimum CW-pumped FWM performance, which does not depend on the dispersion slope, may be achieved for high-slope HNLFs. Conversely, a large pulsed-pump FWM bandwidth is highly dependent on a low slope. Hence, it is important to choose a fiber optimized for a specific application, which is likely different depending on whether a CW- or pulsed-pump is required.

Funding. The Danish Council for Independent Research (DFF) Sapere Aude Advanced Grant, NANO-SPECs (DFF-4005-00558B).

References

1. K. Inoue, J. Lightw. Technol. **10**, 1553 (1992).
2. J. Hansryd, P. A. Andrekson, M. Westlund, J. Li and P.-O. Hedekvist, IEEE J. Sel. Topics Quantum Electron. **8**, 506 (2002).
3. S. Watanabe and M. Shirasaki, J. Lightw. Technol. **14**, 243 (1996).
4. I. D. Philips, M. Tan, M. F. Stephens, M. McCarthy, E. Giacoumidis, S. Sygletos, P. Rosa, S. Fabbri, S. T. Le, T. Kanesan, S. K. Turitsyn, N. J. Doran, P. Harper and A. D. Ellis, in *Optical Fiber Communication Conference* (2014), paper M3C.1.
5. H. Sunnerud, M. Westlund, Mats Sköld and P. A. Andrekson, in *Optical Fiber Communication Conference* (2009), paper OThF4.
6. M. Nakazawa, T. Hirooka, F. Futami and S. Watanabe, IEEE Photon. Technol. Lett. **16**, 1059 (2004).
7. P. Guan, K. M. Røge, H. C. H. Mulvad, M. Galili, H. Hu, M. Lillieholm, T. Morioka, L. K. Oxenløwe, J. Lightw. Technol. **34**, 626 (2016).
8. B. H. Kolner, J. Quantum Electron. **30**, 1951 (1994).
9. T. Torounidis, P. A. Andrekson and B.-E. Olsson, IEEE Photon. Technol. Lett. **18**, 1194 (2006).
10. E. Myslivets, C. Lundström, J. M. Aparicio, S. Moro, A. O. J. Wiberg, C.-S. Bres, N. Alic, P. A. Andrekson and S. Radic, IEEE Photon. Technol. Lett. **21**, 1807 (2009).

11. M. E. Marhic, N. Kagi, T.-K. Chiang and L. G. Kazovsky, Opt. Lett. **21**, 573 (1996).
12. M. E. V. Pedersen, T. Pálsson, K. G. Jespersen, D. Jakobsen, B. Pálsdóttir and K. Rottwitt, in *Proceedings of IEEE Photonic Society 24th Annual Meeting* (IEEE, 2011), p. 571.
13. B. P.-P. Kuo, J. M. Fini, L. Grüner-Nielsen and S. Radic, Opt. Express **20**, 18611 (2012).
14. C. R. Menyuk, J. Eng. Math **36**, 113 (1999).
15. C. J. McKinstrie, H. Kogelnik, R. M. Jopson, S. Radic and A. V. Kanaev, Opt. Express **12**, 2033 (2004).
16. H. Hu, D. Kong, E. Palushani, J. D. Andersen, A. Rasmussen, B. M. Sørensen, M. Galili, H. C. H. Mulvad, K. J. Larsen, S. Forchhammer, P. Jeppesen and L. K. Oxenløwe, in *Conference on Lasers and Electro-Optics 2013* (Optical Society of America, 2013), paper CTh5D.5.
17. L. G. Cohen, W. L. Mammel and S. Lumish, IEEE J. Quantum Electron. **18**, 49 (1982).
18. S. K. Korotky, P. B. Hansen, L. Eskildsen and J. J. Veselka, in *Integrated Optics and Optical Fiber Communications* **2** (IOOC 1995), paper WD2.
19. L. S. Rishøj and K. Rottwitt, in *Nonlinear Photonics Technical Digest 2010* (Optical Society of America, 2010), paper NTuC11.
20. J. Hult, J. Lightw. Technol. **25**, 3770 (2007).
21. A. M. Heidt, J. Lightw. Technol. **27**, 3984 (2009).
22. Q. Lin and G. P. Agrawal, Opt. Lett. **31**, 3086 (2006).
23. M. Karlsson, J. Opt. Soc. Am. B **15**, 2269 (1998).